25th ABCM International Congress of Mechanical Engineering
October 20-25, 2019, Uberlândia, MG, Brazil

SYNCHRONIZATION ANALYSIS OF TWO CLUSTERS OF OSCILLATORS CONNECTED BY SHAPE MEMORY ALLOY RESTORING ELEMENTS

Paula de Arruda Cardoso
Alberto Paiva
Alex Neves Brandão Mendes
Universidade Federal Fluminense – Volta Redonda School of Engineering – Department of Mechanical Engineering
420 Trabalhadores Av. – Volta Redonda – RJ – Brazil – 27.255-250
e-mails: paula.arruda.cardoso@hotmail.com; albertopaiva@id.uff.br; alexbrandao@id.uff.br

Marcelo Amorim Savi
Universidade Federal do Rio de Janeiro – COPPE – Department of Mechanical Engineering
Center for Nonlinear Mechanics – MECANON – Rio de Janeiro – RJ – Brazil – 21.941.972
e-mail: savi@mecanica.ufrj.br

Abstract. *Dynamical systems synchronization study has been prompted in the last decades, due to the growing interest in understanding the regulatory mechanisms that rule this kind of behavior, which arises in natural systems, as well as in mechanical systems. This work deals with dynamical modeling and numerical simulation of a mechanical system comprising two platforms connected in series by linear restoring and damping elements. Each platform supports two pendula, such that each pair of pendula is connected by a shape memory alloy restoring element. The system encompasses six degrees of freedom and the differential equations of motion are solved by a fourth-order Runge-Kutta method. The system natural behavior is investigated by means of maps involving different sets of initial conditions for the pendula, varying the platforms damping parameter and the shape memory restoring elements temperature. Numerical results include situations where the system loses/embodies synchronization, characterizing different types of behavior for the system elements - platforms and pendula fully synchronized, partially synchronized (in-phase/anti-phase), desynchronized and rest.*

Keywords: *Nonlinear dynamics, synchronization, shape memory alloy, numerical simulation.*

1. INTRODUCTION

Intuitively, synchronization may be understood as a process in which different oscillators fit their behavior reciprocally, exhibiting a collective performance. Synchronization phenomena are present either in natural/biological/chemical systems or in mechanical archetypes and its occurrence is usually driven by some kind of coupling among the oscillators. The motivation to study this subject lies upon the possibility of controlling the system response to achieve a specific desired behavior. For instance, in mechanical systems, a feasible possibility is to synchronize a cluster of rotating oscillators for energy harvesting purpose.

The study of synchronizing systems may be considered somewhat recent. A milestone in this subject is the work conducted by Kuramoto (1975) that proposed a nonlinear equation to represent the behavior of a cluster with a large (but finite) number of coupled oscillators. Some other authors have been using Kuramoto's equation to model different phenomena (Martens et al. 2009; O'Keeffe et al. 2017; Loffler & Strogatz, 2018). Some other authors focus on different formulations for particular mechanical systems. Pantaleone (2002) studied a system composed by a platform supported by two idlers, holding two metronomes. He inferred that no matter the initial conditions, after a transient, the metronomes synchronize, preferentially in phase. Koluda et al. (2014) dealt with the numerical simulation of a mass-spring-damper system supporting two double pendula, which may be externally excited. They investigated the possible shape modes after synchronization.

More recently, the same precursor researcher on the subject – Yoshiki Kuramoto – identified a very particular behavior presented by identical oscillators symmetrically arranged, in which one cluster of oscillators behave synchronized, while others remain asynchronous, under specific input conditions. Later, this behavior pattern was named as "chimera state" (Abrams & Strogatz, 2004). Panaggio & Abrams (2015) present a review work, dealing with both topology and synchronization features of different oscillatory systems. Wojewoda et al. (2016) investigate the simplest arrangement to achieve the chimera state. He conducts an experimental/numerical analysis, concerning three metronomes with their pivoting points forming an equilateral triangle, with their rods coupled by linear restoring/damping elements. There are other relevant works on the subject, including recent experimental works.

This paper deals with the mathematical modeling and numerical simulation, focusing on a synchronization analysis of a specific mechanical system that will be better explained in the following section.

2. PHYSICAL MODEL AND EQUATIONS OF MOTION

This section presents both the physical model and the summarized dimensionless equations of motion for the mechanical system. Figure 1 illustrates the physical model, where both bases (namely: bases B1 and B2) translate along *y* direction without friction. Base B1 supports two pendula (namely: pendula P1 and P2) that constitute the first cluster of oscillators; analogously, base B2 supports pendula P3 and P4 related to the second cluster. Pendula P1 and P2 are interconnected by an **SMA** restoring element (namely, SMA1 element), while pendula P3 and P4 are linked by the SMA2 element.

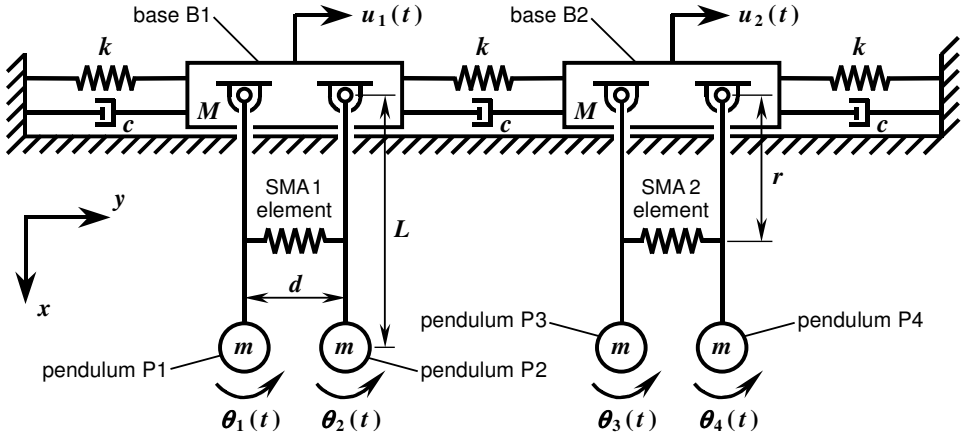

Figure 1. Physical model.

The system presents six degrees of freedom, being two of them associated with the bases' translation – $u_1(t)$ and $u_2(t)$ for bases B1 and B2, respectively; and $\theta_1(t)$, $\theta_2(t)$, $\theta_3(t)$ and $\theta_4(t)$ for pendula P1, P2, P3 and P4, while *t* is the independent variable time. Concerning the constant system parameters, *M* and *m* are the masses of each base and of each pendulum, respectively; *k* and *c* are the stiffness and damping coefficients for the linear springs and dashpots attached to the bases, respectively; the distances *L*, *r* and *d* refer to: the pendula rod length (assumed rigid and massless), the distance between each pendula pivoting point and the **SMA** element attaching point and the distance between the pivoting points of both pendula belonging to the same cluster. It is worthwhile to notice the system symmetry concerning the spatial distribution of its several elements.

The **SMA** elements are considered equal bars undergoing tension/compression; thus, the total strain energy potential U_i (i = 1, 2) for each of the **SMA** elements is given by:

$$U_i = \psi_i \, V_{\mathrm{SMA}} = \psi_i \, L_{\mathrm{SMA}} \, A_{\mathrm{SMA}} \tag{1}$$

where: ψ_i is the free energy potential per unit volume for each element, while V_{SMA}, L_{SMA} and A_{SMA} are the volume, the length and the cross-sectional area of both elements, respectively.

In order to describe the **SMA** thermomechanical behavior, the polynomial constitutive model proposed by Falk (1980) is incorporated into the dynamical model, whose *Helmholtz* free energy potential is stated below in Eq. (2), where: ε_i and T_i are the state variables related to axial strain and absolute temperature, while α, β and γ are material parameters; T_M is the trigger temperature for martensite formation; while T_A is analogous for austenite formation.

$$\psi_i(\varepsilon_i, T_i) = \frac{\alpha(T_i - T_M)}{2}\varepsilon_i^2 - \frac{\beta}{4}\varepsilon_i^4 + \frac{\gamma}{6}\varepsilon_i^6 \qquad \text{where: } \gamma = \beta^2 / 4\alpha(T_A - T_M) \tag{2}$$

Figure 2 presents a disturbed condition of pendula P1and P2, in order to evaluate the SMA1 bar elongation that enables its strain determination that, finally, results in the associated total strain energy potential expression.

Considering the SMA1 bar axial strain as: $\varepsilon_1 = \Delta L / L_{\mathrm{SMA}}$, where ΔL is its axial elongation given by: $\Delta L = \sqrt{b^2 + h^2} - d$, while $L_{\mathrm{SMA}} = d$. The distances *b* and *h* may be identified from Fig. (2) as follows:

$$b = d + r\sin\theta_2 - r\sin\theta_1 \qquad \text{and} \qquad h = r\cos\theta_1 - r\cos\theta_2 \tag{3}$$

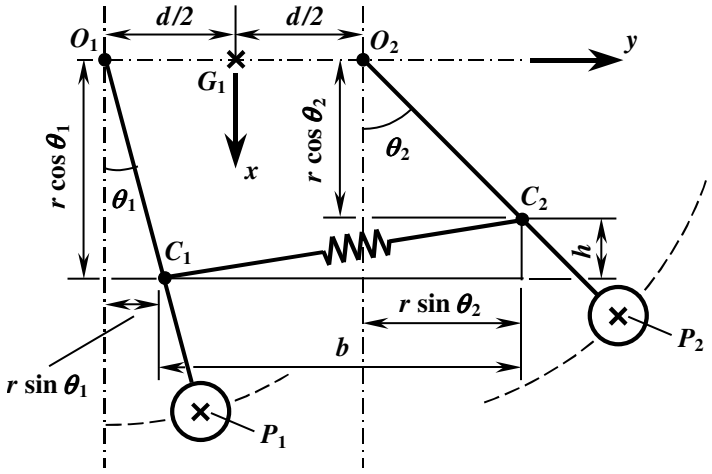

Figure 2. Disturbed condition of pendula P1 and P2.

Regarding these quantities (b and h), it is possible to set:

$$\lambda^2 = b^2 + h^2 = d^2 + 2r^2 + 2d\,r\left(\sin\theta_2 - \sin\theta_1\right) - 2r^2\cos\left(\theta_2 - \theta_1\right) \tag{4}$$

Therefore, for the SMA1 element, the bar elongation and the according strain are, respectively, obtained as:

$$\Delta L = \lambda - d \qquad \text{and} \qquad \varepsilon_1 = \frac{\lambda - d}{d} \tag{5}$$

Analogously, elongation and axial strain for the SMA2 element are, respectively:

$$\Delta L_* = \lambda_* - d \qquad \text{and} \qquad \varepsilon_2 = \frac{\lambda_* - d}{d} \tag{6}$$

where, now, λ_* is defined as:

$$\lambda_*^2 = d^2 + 2r^2 + 2d\,r\left(\sin\theta_4 - \sin\theta_3\right) - 2r^2\cos\left(\theta_4 - \theta_3\right) \tag{7}$$

Finally, the total strain energy potential for SMA1 and SMA2 elements, respectively, provides:

$$\begin{aligned} U_1\left(\theta_1,\theta_2\right) &= \left\{ \frac{\alpha\left(T_1 - T_M\right)}{2}\left[\frac{\lambda - d}{d}\right]^2 - \frac{\beta}{4}\left[\frac{\lambda - d}{d}\right]^4 + \frac{\gamma}{6}\left[\frac{\lambda - d}{d}\right]^6 \right\} d\,A_{\text{SMA}} \quad \Rightarrow \text{for SMA1 element} \\ U_2\left(\theta_3,\theta_4\right) &= \left\{ \frac{\alpha\left(T_2 - T_M\right)}{2}\left[\frac{\lambda_* - d}{d}\right]^2 - \frac{\beta}{4}\left[\frac{\lambda_* - d}{d}\right]^4 + \frac{\gamma}{6}\left[\frac{\lambda_* - d}{d}\right]^6 \right\} d\,A_{\text{SMA}} \quad \Rightarrow \text{for SMA2 element} \end{aligned} \tag{8}$$

The total strain energy potential expressions are derived here, since they are of special interest, while exploring the numerical results. For the sake of conciseness, other energy/work terms are omitted here. For further details about the complete Lagrangian formulation to obtain the equations of motion, please refer to Cardoso (2019).

At this point, new dimensionless variables are defined as follows: $\tau = \omega t$ is the new independent variable (dimensionless time), while ω is a reference frequency set as $\omega = \sqrt{k/(M+2m)}$; $X_i = u_i / L$ (for $i = 1, 2$) are the new dimensionless bases' displacements; the pendula angular displacements (θ_j for j = 1, 2, 3, 4) are already dimensionless. The derivative $(\,)' = d(\,)/d\tau$ represents the ordinary differentiation of the new dependent variables (X_i and θ_j) with respect to τ.

Equation (9) presents the new dimensionless system parameters, $\overline{M}$ represents the ratio between the mass of one pendulum and the total mass of a cluster (including the base mass); ξ is the new dimensionless damping parameter; η is related to a (linear) natural frequency of one pendulum alone; $\bar{r}$ is the ratio between the distances r and d; $\overline{\alpha}$, $\overline{\beta}$ and $\overline{\gamma}$ are the new dimensionless **SMA** material parameters and $\overline{T}_i$ (for $i=1,2$) provides the **SMA** elements dimensionless temperatures.

$$\overline{M}=\frac{m}{(M+2m)} \qquad \xi=\frac{c}{(M+2m)\,\omega} \qquad \eta=\frac{g}{L\,\omega_{\text{Ref}}^{2}} \qquad \bar{r}=\frac{r}{d}$$
$$\overline{\alpha}=\frac{\alpha\, T_M\ \bar{r}\, d\, A_{\text{SMA}}}{m\, L^2\ \omega^2} \qquad \overline{\beta}=\frac{\beta\, \bar{r}\, d\, A_{\text{SMA}}}{m\, L^2\ \omega^2} \qquad \overline{\gamma}=\frac{\gamma\, \bar{r}\, d\, A_{\text{SMA}}}{m\, L^2\ \omega^2} \qquad \overline{T}_i=\frac{T_i}{T_M} \tag{9}$$

Chart 1 displays the six dimensionless equations of motion for the proposed physical model, as follows. Concerning the numerical procedure, these equations of motion are numerically integrated by the fourth-order *Runge-Kutta* method. In parallel, a brute force handmade algorithm is developed, in order to classify the type of synchronism of the pendula behavior, by real time monitoring and comparison of the time evolution of the pendula displacements.

Chart 1. Equations of motion.

$$X_1''+\overline{M}\left(\theta_1''\cos\theta_1+\theta_2''\cos\theta_2\right)-\overline{M}\left(\theta_1'^{\,2}\sin\theta_1+\theta_2'^{\,2}\sin\theta_2\right)+2\,\xi\,X_1'-\xi\,X_2'+2\,X_1-X_2=0$$

$$X_2''+\overline{M}\left(\theta_3''\cos\theta_3+\theta_4''\cos\theta_4\right)-\overline{M}\left(\theta_3'^{\,2}\sin\theta_3+\theta_4'^{\,2}\sin\theta_4\right)-\xi\,X_1'+2\,\xi\,X_2'-X_1+2\,X_2=0$$

$$X_1''\cos\theta_1+\theta_1''-\left[\cos\theta_1+\bar{r}\sin\left(\theta_2-\theta_1\right)\right]\left\{\overline{\alpha}\left(\overline{T}_1-1\right)\left[\frac{\overline{\lambda}-1}{\overline{\lambda}}\right]-\overline{\beta}\left[\frac{\left(\overline{\lambda}-1\right)^3}{\overline{\lambda}}\right]+\overline{\gamma}\left[\frac{\left(\overline{\lambda}-1\right)^5}{\overline{\lambda}}\right]\right\}+\eta\sin\theta_1=0$$

$$X_1''\cos\theta_2+\theta_2''+\left[\cos\theta_2+\bar{r}\sin\left(\theta_2-\theta_1\right)\right]\left\{\overline{\alpha}\left(\overline{T}_1-1\right)\left[\frac{\overline{\lambda}-1}{\overline{\lambda}}\right]-\overline{\beta}\left[\frac{\left(\overline{\lambda}-1\right)^3}{\overline{\lambda}}\right]+\overline{\gamma}\left[\frac{\left(\overline{\lambda}-1\right)^5}{\overline{\lambda}}\right]\right\}+\eta\sin\theta_2=0$$

$$X_2''\cos\theta_3+\theta_3''-\left[\cos\theta_3+\bar{r}\sin\left(\theta_4-\theta_3\right)\right]\left\{\overline{\alpha}\left(\overline{T}_2-1\right)\left[\frac{\overline{\lambda}_*-1}{\overline{\lambda}_*}\right]-\overline{\beta}\left[\frac{\left(\overline{\lambda}_*-1\right)^3}{\overline{\lambda}_*}\right]+\overline{\gamma}\left[\frac{\left(\overline{\lambda}_*-1\right)^5}{\overline{\lambda}_*}\right]\right\}+\eta\sin\theta_3=0$$

$$X_2''\cos\theta_4+\theta_4''+\left[\cos\theta_4+\bar{r}\sin\left(\theta_4-\theta_3\right)\right]\left\{\overline{\alpha}\left(\overline{T}_2-1\right)\left[\frac{\overline{\lambda}_*-1}{\overline{\lambda}_*}\right]-\overline{\beta}\left[\frac{\left(\overline{\lambda}_*-1\right)^3}{\overline{\lambda}_*}\right]+\overline{\gamma}\left[\frac{\left(\overline{\lambda}_*-1\right)^5}{\overline{\lambda}_*}\right]\right\}+\eta\sin\theta_4=0$$

The dimensionless parameters $\overline{\lambda}$ and $\overline{\lambda}_*$ have to do with the axial elongation of the **SMA** bars SMA1 and SMA2, respectively, whose expressions are given below by Eq. (10).

$$\overline{\lambda}^{\,2}=1+2\,\bar{r}^{\,2}+2\,\bar{r}\left(\sin\theta_2-\sin\theta_1\right)-2\,\bar{r}^{\,2}\cos\left(\theta_2-\theta_1\right) \quad \text{and}$$
$$\overline{\lambda}_*^{\,2}=1+2\,\bar{r}^{\,2}+2\,\bar{r}\left(\sin\theta_4-\sin\theta_3\right)-2\,\bar{r}^{\,2}\cos\left(\theta_4-\theta_3\right) \tag{10}$$

The dimensionless total strain energy potential for SMA1 and SMA2 elements provides, respectively:

$$\overline{U}_1\left(\theta_1,\theta_2\right)=\frac{\overline{\alpha}\left(\overline{T}_1-1\right)}{2\,\bar{r}}\left[\overline{\lambda}-1\right]^2-\frac{\overline{\beta}}{4\,\bar{r}}\left[\overline{\lambda}-1\right]^4+\frac{\overline{\gamma}}{6\,\bar{r}}\left[\overline{\lambda}-1\right]^6 \quad \Rightarrow \text{for SMA1 element}$$
$$\overline{U}_2\left(\theta_3,\theta_4\right)=\frac{\overline{\alpha}\left(\overline{T}_2-1\right)}{2\,\bar{r}}\left[\overline{\lambda}_*-1\right]^2-\frac{\overline{\beta}}{4\,\bar{r}}\left[\overline{\lambda}_*-1\right]^4+\frac{\overline{\gamma}}{6\,\bar{r}}\left[\overline{\lambda}_*-1\right]^6 \quad \Rightarrow \text{for SMA2 element} \tag{11}$$

while the dimensionless elongation for SMA1 and SMA2 elements are, respectively, given by:

$$\overline{\Delta L} = \overline{\lambda} - 1 \qquad \text{and} \qquad \overline{\Delta L}_{*} = \overline{\lambda}_{*} - 1 \tag{12}$$

3. NUMERICAL RESULTS

This section presents numerical results for the natural behavior of the proposed system. Firstly, an equilibrium point analysis is performed for different **SMA** elements temperature ranges. Equal temperatures are adopted for both SMA1 and SMA2 elements, during all simulations; thus: $\overline{T}_1 = \overline{T}_2 = \overline{T}$. Then, attempting to analyze both synchronization patterns – within and between clusters, colormaps scanning initial conditions are evaluated, considering variation of two parameters: the bases damping coefficient and the **SMA** elements temperature. Table 1 exhibits the dimensionless parameters values used along the simulations, except for those that are varied.

Table 1. Dimensionless parameters values for numerical simulations.

$\overline{M}$	$\overline{r}$	η	$\overline{\alpha}$	$\overline{\beta}$	$\overline{\gamma}$
0.150	0.200	0.300 x 10³	2.060 x 10³	15.800 x 10³	0.010 x 10³

Figure 3 presents an equilibrium point analysis for a conservative condition ($\xi = 0$), classifying their nature, for the three typical temperature ranges of the **SMA** elements, namely: low temperature ($\overline{T} = 0.99 < \overline{T}_M$); intermediate temperature ($\overline{T}_M < \overline{T} = 1.12 < \overline{T}_A$) and high temperature ($\overline{T} = 1.27 > \overline{T}_A$), where: $\overline{T}_M = 1$ and $\overline{T}_A \cong 1.22$. The results show phase portraits and **SMA** strain energy potentials for each temperature.

From literature, it is well known that, in a mechnical system, the concept of equilibrium point implies null (linear and angular) velocities and accelerations. By neglecting all terms present in the six equations of motion, displayed in Chart 1, involving $X_i^{'}$ and $X_i^{''}$ (for $i = 1, 2$), as well as $\theta_j^{'}$ and $\theta_j^{''}$ (for $j = 1, 2, 3, 4$), it is possible to infer that the bases should remain at rest, during the equilibrium point analysis. Therefore, the system behaves such that the two clusters are decoupled. Moreover, for each pendulum, the equilibrium condition takes place when there is a balance between the moments generated by the **SMA** element restoring force and the weight force.

Figures 3(a), 3(c) and 3(e) show phase portraits for the three temperatures range cited above; accordingly, Figs. 3(b), 3(d) and 3(f) illustrate the respective **SMA** strain energy potentials. For this equilibrium point analysis, since the bases should not move, only symmetric displacement initial conditions (same amplitude with opposite signs) are adopted for each pendulum of both clusters. The velocity initial conditions are all null. Due to the symmetry of the pendula behavior, only the P1 pendulum response is presented in the phase portraits (state subspace $\theta_1 \times \dot{\theta}_1$) and only the SMA1 restoring element strain energy potential is evaluated.

Regarding the phase portraits, it is possible to identify some mixed similarities with both the simple pendulum phase portarait and the spring-mass oscilator using *Falk*'s model. From the dynamical point of view, a curious fact concerns the dynamical complexity increase for low and high temperatures, while compared with the spring-mass oscilator using *Falk*'s model, which provides the richest dynamical response for the intermediate temperature. The homoclinic orbits are assigned in bold lines in the phase portraits.

Now, observing SMA1 restoring element strain energy potentials, it is clearly possible to identify not only an increase in the number of equilibrium points but also some shift in their positions, compared to the typical equilibrium points present in the *Falk* model strain energy potentials. This feature is related to the gravitational effect combined with the nonlinear effects of the **SMA** element behavior, enabling non-intuitive equilibrium points.

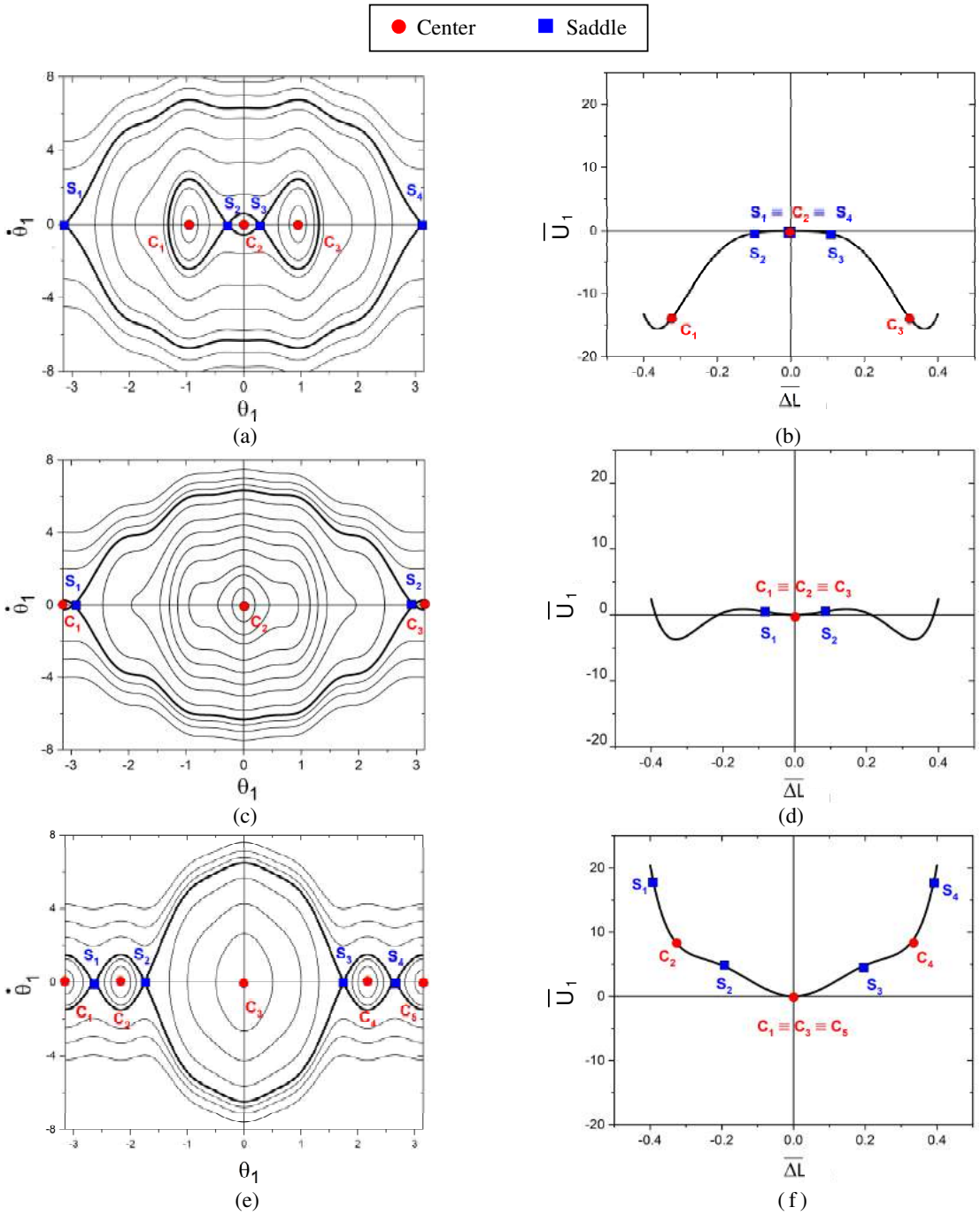

Figure 3. Equilibrium point analysis for three different **SMA** elements temperature ranges.

	Phase portrait	**SMA** strain energy potential
Low temperature	(a)	(b)
Intermediate temperature	(c)	(d)
High temperature	(e)	(f)

Figure 4 shows synchronization maps involving four values of the damping coefficients: $\xi = 0$ (without dmping); $\xi = 0.01$; $\xi = 0.1$ and $\xi = 1$; and three different temperatures, as set for the previous results. Regarding the applied initial conditions, only the pendula displacements are non-null and equal initial conditions amongst the clusters (*i.e.*: $\theta_1 = \theta_3$ and $\theta_2 = \theta_4$) are adopted.

Collectively observing the synchronization maps, it is possible to verify that both parameters (bases damping coefficient and **SMA** elements temperature), while increased, are responsible for the basins erosion. The synchronization classification migrates from a former condition (without damping) – asynchronous within the clusters and in-phase between clusters; passing by a condition – anti-phase within the clusters and asynchronous between clusters – for intermediate damping values; tending to a condition anti-phase within the clusters and in-phase between clusters – for high damping values.

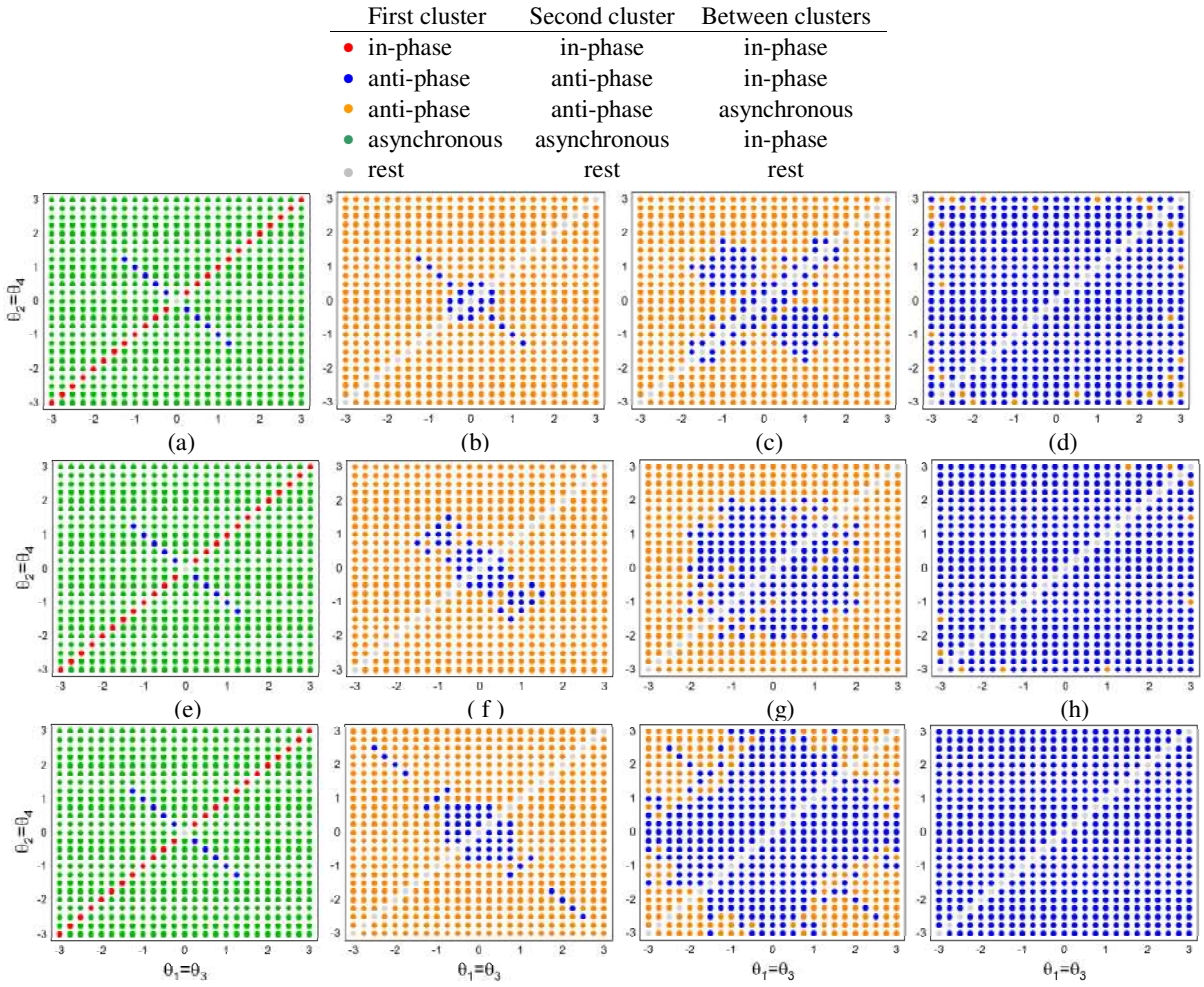

Figure 4. Synchronization maps for equal initial conditions amongst the clusters varying the bases damping coefficient and the **SMA** elements temperature.

	$\xi = 0$	$\xi = 0.01$	$\xi = 0.1$	$\xi = 1$
Low temperature	(a)	(b)	(c)	(d)
Intermediate temperature	(e)	(f)	(g)	(h)
High temperature	(i)	(j)	(k)	(l)

4. CONCLUDING REMARKS

This paper deals with the numerical simulation of a mechanical system comprising two clusters of oscillators connected by shape memory alloy restoring elements, with the purpose of scrutinizing synchronization patterns. Initially, an equilibrium point analysis varying the **SMA** temperature helps understanding the system dynamics, in order to better interpret the synchronization results. The results reveal an increase in the typical number of equilibrium points, some of them out of their intuitive positions, due to the gravitational effect combined with the nonlinear effects of the **SMA** elements behavior. Besides that, lower and higher temperatures present the richest dynamical response, instead of the intermediate temperature (usually, the most complex, for *Falk*'s model). Concerning the synchronization analysis, the natural behavior is investigated, by means of displacement state subspaces, considering equal initial conditions among the two clusters. During the simulations, two parameters are varied: the bases damping coefficient and the **SMA** elements temperature. For the system without damping, asynchronous behavior prevails, regardless of the **SMA** temperature. After the damping inclusion, both parameters, while increased, favor pendula synchronization in anti-phase (180º lagged) within the clusters and in phase between clusters.

5. REFERENCES

Abrams, D.M.; Strogatz, S.H.; 2004; "Chimera States for Coupled Oscillators"; Physical Review Letters; Vol. 93 Article ID: 174102.

Falk, F.; 1980; "Model Free-Energy, Mechanics and Thermodynamics of Shape Memory Alloys"; ACTA Metallurgica; Vol. 28; pp. 1773-1780.

Koluda, P.; Perlikowski, P.; Czolczynski, K.; Kapitaniak, T.; 2014; "Synchronization Configurations of Two Coupled Double Pendula"; Communications in Nonlinear Science and Numerical Simulation; Vol. 19; pp. 977-990.

Kuramoto, Y.; 1975; "Self-entrainment of a Population of Coupled Nonlinear Oscillators"; In H. Araki Ed.; International Symposium on Mathematical Problems in Theoretical Physics; pp. 420-422; Berlin; Springer.

Loffler, B.O.; Strogatz, S.H.; 2018; "Kuramoto Model with Uniformly Spaced Frequencies: Finite-N Asymptotics of the Locking Threshold"; Physical Review; 2018.

Martens, E.A.; Barreto, E.; Strogatz, S.H.; Ott, E.; Antonsen, T.M.; 2009; "Exact Results for the Kuramoto Model with a Bimodal Frequency Distribution"; Physical Review; Vol 79; 11 pp.

Najdecka, A., Kapitaniak, T., Wiercigroch, M.; 2015; "Synchronous Rotational Motion of Parametric Pendulums"; International Journal of Non-Linear Mechanics; Vol. 70; pp. 84-94.

O'Keeffe, K.P., Hong, H., Strogatz, S.H.; 2017; "Oscillators that Sync and Swarm"; Nature Communications; Vol. 8; 13 pp.

Panaggio, M.J.; Abrams, D.M.; 2015; "Chimera States: Coexistence of Coherence and Incoherence in Networks of Coupled Oscillators"; London Mathematical Society; Vol. 28; pp. 67-87.

Pantaleone, J.; 2002; "Synchronization of Metronomes"; American Assoc. of Physics Teachers; Vol. 70; pp. 992-1000.

Wojewoda, J.; Czolczynski, K.; Maistrenko, K.; Kapitaniak, T.; 2016; "The Smallest Chimera State for Coupled Pendula"; Scientific Reports; Vol. 6; Article ID: 34329.

6. RESPONSIBILITY NOTICE

The authors are the only responsible for the printed material included in this paper.